INTERNATIONAL JOURNAL OF HYDROGEN ENERGY 49 (2024) 968–979

Available online at www.sciencedirect.com

ScienceDirect

journal homepage: www.elsevier.com/locate/he

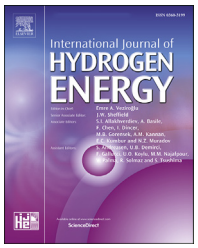

Comprehensive analysis on the effect of lube oil on particle emissions through gas exhaust measurement and chemical characterization of condensed exhaust from a DI SI engine fueled with hydrogen. Part 2: Effect of operating conditions

Barbara Apicella, Francesco Catapano, Silvana Di Iorio, Agnese Magno[*], *Carmela Russo, Paolo Sementa, Antonio Tregrossi, Bianca Maria Vaglieco*

Institute of Science and Technology for Sustainable Energy and Mobility (STEMS) - CNR, Napoli, Italy

HIGHLIGHTS

- Physical and chemical characterization of particles emitted by a SI engine fueled with hydrogen.
- Role of lubricating oil on the mechanisms of particle formation for hydrogen fueling.
- Impact of the operating condition, engine speed and load, on the particles emitted by a hydrogen-fueled SI engine.
- Presence of PAH, alkyl-PAHs, oxy-PAHs and nanoparticles in the exhausts.
- Soot formation at higher engine speed.

ARTICLE INFO

Article history:
Received 25 July 2023
Received in revised form
22 September 2023
Accepted 26 September 2023
Available online 10 October 2023

Keywords:
Hydrogen
Particle emission
Lube oil
PAH
Spark ignition engine

ABSTRACT

The need to cope with carbon dioxide abatement has prompted the development of innovative technologies for sustainable mobility. Meanwhile, these technologies consolidate, an important role will be played by internal combustion engines fed with non-fossil fuels such as hydrogen. Theoretically, the combustion of hydrogen should not produce carbon-based emissions. Nevertheless, particles can be found in the exhaust of hydrogen-fueled engines because of the lubricating oil. In this study, a thorough examination of the impact of the engine lubricant on the mechanisms leading to the formation of the particles and the high levels of hazardous pollutants was performed in this study. Experiments were carried out on a direct injection spark ignition engine fueled with hydrogen. The analysis was conducted at 2000 and 3000 rpm both low and full load. Number and size particle distribution were determined by means of on-line measurement on the diluted exhaust. Off-line chemical characterization through analytic techniques was realized on the condensed exhaust and on the particles collected on a filter. Experimental results pointed out that the extent of the particle size varies according to the engine speed and load, evidencing the different role of the oil ascribable to the environmental conditions. It was found that aromatic molecules and

* *Corresponding author*. Institute of Science and Technology for Sustainable Energy and Mobility (STEMS), Via G. Marconi 4, 80125 Naples, Italy.
E-mail address: agnese.magno@stems.cnr.it (A. Magno).

https://doi.org/10.1016/j.ijhydene.2023.09.279

nanoparticles are present in the exhausts at all the investigated operating conditions, whereas soot aggregates are formed only at high engine speed.

1. Introduction

The climate and green growth strategy of the European Union set the objective of achieving net-zero greenhouse gas emissions by 2050. Electric powertrain systems have been proposed to pursue climate neutrality [1]. However, the adoption of low/zero carbon fuels such as ammonia, methanol, e-fuels, methane and hydrogen could help to reach the target of carbon dioxide (CO_2) reduction without completely banning internal combustion engines (ICEs).

Alcohols such as ethanol and methanol have long been the main alternative fuels for spark ignition (SI) engines thanks to their renewable nature and effective role in reducing pollutant emissions [2–4]. Moreover, they benefit from facility of transportation and storage compared to gaseous fuels [5].

Recently, great attention has been paid to gaseous fuels due to their capability to drastically reduce the pollutant emissions [6]. Hydrogen as a fuel for road transport has, in fact, good potential to support the zero-carbon energy strategies [7]. In the last years, it was the object of several research studies for its application in the fuel cells and less interest was devoted to its use in ICEs [8]. Nevertheless, traditional propulsion systems can be customized to operate with pure hydrogen representing a more robust and less expensive solution [9]. Hydrogen is an attractive alternative fuel for SI engines due to its properties [10]. It has low ignition energy that guarantees stable combustion and good behavior at cold start operation. It is characterized by high laminar burning velocity resulting in low cycle-to-cycle variation. However, it suffers from some drawbacks such as power reduction and safety issues due to preignition and backfire [11].

Existing literature exploring the opportunities and challenges of hydrogen-fueled SI engines was mainly focused on the port fuel injection (PFI) method [12]. This solution guarantees a well premixed charge thus resulting in reduced emissions. On the other hand, this technology can lead to abnormal combustion and power loss. Hydrogen direct injection (DI) strategy can be applied to compensate for the low volumetric efficiency and resolve the backfire issue [13]. Despite the DI ICE fueled by hydrogen has great potential, its performance and emissions, especially particle emissions, were not sufficiently explored. It is well known that gasoline DI is characterized by high particle emissions because of the wall-wetting effect and the reduced time for fuel evaporation and mixing with air thus resulting in an inhomogeneous charge formation [14]. For gaseous fuels DI injection the mechanisms of the particle formation are different since a pivotal role is played by the lubricating oil [15]. Studies on the effect of the lubricating oil on particulate emission in diesel [16,17] and gasoline [18] vehicles have highlighted their contribution mainly to organic carbon [19,20] and sub-23 nm [21] particles leading for the development of new oil formulation [22]. To the best of author knowledge, few papers are available in literature on the effect of pure hydrogen on particle emission. Singh et al. [23] carried out an experimental investigation to compare the characteristics of the particulate emission from mineral diesel, gasoline, compressed natural gas (CNG), hydrogen-CNG mixtures (HCNG) and hydrogen-fueled engines. Tests with gaseous fuels were carried out on a compression ignition engine modified to operate in SI mode in which the fuel was port injected. They observed that in the case of hydrogen fueling, incomplete combustion of lubricating oil present on the cylinder walls and its pyrolysis during the post-combustion reactions result in a significant number of particles.

Thawko et al. [24] performed a comparative experimental analysis of the performance and emissions, including particles, of a diesel engine modified to allow SI DI operation with the gaseous fuel. The engine was fed with hydrogen, hydrogen-rich reformate and methane. They noticed that the hydrogen low flame quenching distance leads to enhanced lubricant evaporation with the subsequent particle formation under high engine loads.

In another study, Thawko et al. [25] showed that non-premixed hydrogen combustion leads to a large particle formation even higher than that from hydrocarbon fuels. This is due to the combination of two effects that are the lower flame quenching distance that intensifies lubricant evaporation and the interaction between the lubricant vapor and the core jet. Consequently, there is an excessive entrainment of lubricant vapor into the chamber that is involved in the combustion process.

Although the presence of particles in the exhaust of hydrogen-fueled engines is highlighted in literature, the mechanisms, such as oxidation and dissociation, involved in the oil transformation and, hence, responsible for the formation of the particle are not fully investigated.

The present study aims to fill this gap by proposing a comprehensive investigation on the contribution of the lubricating oil on the emission of particles from a pure hydrogen-fueled single cylinder, 250 cm^3 DI SI engine. This study follows the already published paper from the authors [15] where the mechanisms of particle formation due to the lubricating oil contribution from a DI SI engine fueled with hydrogen were investigated. The novelty of the present work consists in analyzing the role of the different environmental conditions occurring at different engine speed and load on the processes of particle formation involving the lubricating oil. For this purpose, the investigation was performed at four operating conditions, at 2000 and 3000 rpm both low (LL) and high load (HL), chosen as representative of urban and extra-

urban driving conditions. Particles were characterized on-line in terms of number and size through an Engine Exhaust Particle Sizer (EEPS) coupled to a single diluter (SD). Off-line chemical characterization was carried out through several analytical techniques applied on the condensed exhaust and the particles collected at the tailpipe.

2. Experimental apparatus and methods

2.1. Test engine

The experimental setup consists of a four-stroke, water-cooled, single-cylinder engine whose technical specifications are summarized in Table 1. A schematic of the experimental layout is shown in Fig. 1. The engine is loaded by an electric dynamometer allowing to operate at constant engine speed. The engine has a prototype four-valves cylinder head with a hole for the housing of the DI system between the two intake valves. The spark plug is mounted in the center of a pent roof combustion chamber.

A proper fuel supply system was developed to enable direct injection of hydrogen. A Synerject strata injector designed for the simultaneous injection of air and gasoline was modified to inject gaseous fuels directly in the chamber. For this purpose, the injector was mounted with an adaptor having the same external geometry of the standard GDI injector. The adapter was internally equipped with ducts allowing the injection of hydrogen toward the spark plug [26].

Hydrogen was stored at 200 bar pressures and decompressed to 6.5 bar by a pressure regulator before being injected into the cylinder. A flame arrestor and a pneumatic-actuated valve were installed in the hydrogen supply line to avoid any hazard caused by backfire.

The air-fuel ratio control of the engine was based on a feedback control system using a linear lambda sensor Bosch LSU 4.9 mounted in the exhaust manifold.

The temperatures of the coolant, the lubricating oil, the intake air and the exhaust gas were measured with K-type thermocouples.

An AVL Engine Timing Unit (ETU) multi-channel system was used to manage the ignition and injection parameters of the engine.

An AVL GH12D piezoelectric pressure transducer was used to measure the in-cylinder pressure evolution.

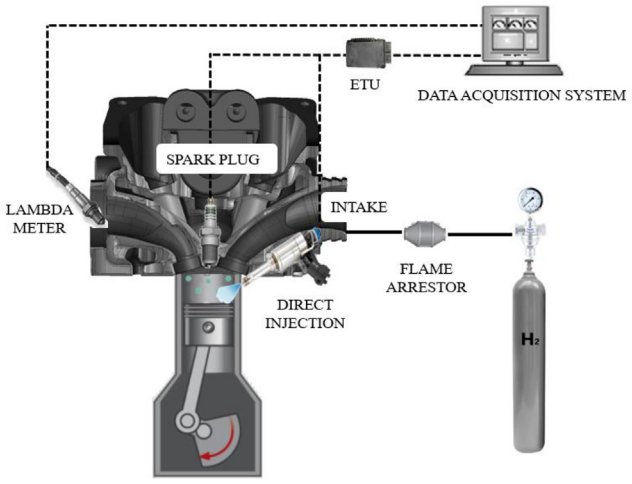

Fig. 1 – Schematic of experimental layout.

A commercial lubricant oil obtained by a combination of synthetic and mineral bases with 10W–40 viscosity grade (Table 2) was used for this study.

2.2. Particle characterization

The experimental layout for particle measurement and sampling is shown in Fig. 2. It consists of an exhaust gas sampling line for physical characterization of the particles in terms of number and diameter. Moreover, it includes two ice-cooled traps to collect condensed species followed by a Teflon filter to accumulate particles for chemical and spectroscopic investigations.

2.2.1. Sampling systems for particle number and size characterization

Accurate and reproducible measurements of particle number and size was carried out by means of the EEPS 3090 from TSI [27]. It measures the particle size distribution (PSD) in the mobility diameter range of 5.6–560 nm up to 10 times per second with a maximum concentration of 10^8 particles/cm^3. It has a size resolution of total 32 channels. At the instrument inlet, there is a cyclone with a 50% cut-size at 1 mm (inlet flowrate 10 lpm). Before entering the EEPS, the exhaust gas sample was taken by a 1.5 m long line heated at 150 °C to prevent water condensation. Then, the sample was diluted through a Dekati single diluter at dilution ratio of 1:9 using filtered air at 150 °C. This system allows to avoid condensation

Table 1 – Engine specifications.

Engine	Spark Ignition
Number of Cylinders	1
Bore [mm]	72
Stroke [mm]	60
Displacement [cm^3]	244.3
Compression Ratio	11.5:1
Max. Power [kW]	16 @ 8000 rpm
Max. Torque [Nm]	20 @ 5500 rpm
Intake	Naturally Aspirated
Injection system	DI Prototype

Table 2 – Lubricant oil properties.

Properties	
Viscosity	10W-40
Density @ 20 °C	0.870 kg/l
Viscosity @ 40 °C	101.7 mm^2/s
Viscosity @ 100 °C	14.5 mm^2/s
Viscosity index	151
Pour point	−35.0 °C
TBN	10.1 mg KOH/g
Flash point	228 °C

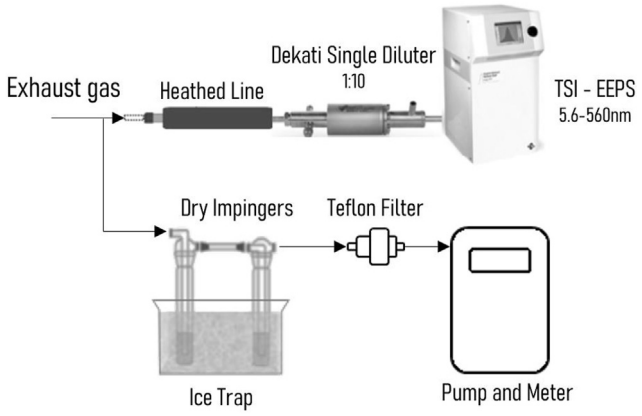

Fig. 2 – Experimental setup for particle measurement and for condensed exhaust sampling.

and nucleation effects thus making the PSD measurement stable and repeatable.

2.2.2. *Sample treatment and chemical and spectroscopic techniques*

The soluble organic fraction (SOF) was recovered cleaning the sampling line, performing a liquid-liquid extraction of condensed water, and isolating the Dichloromethane (DCM)-soluble fraction of the sample collected on the filter. Soot represents the DCM-insoluble component of the condensed exhausts collected along the sampling line. More details on the sampling approach and sample treatments are reported in Ref. [28]. The condensed exhausts were characterized using chemical and spectroscopic methods.

The gas chromatography mass spectrometer (GC-MS) employed is an AGILENT GC 6890 - MSD 5975C. The mass spectrometer operated in electron ionization mode, and *m/z* was scanned from 50 to 400. Using response factors determined from the analysis of standard samples with known quantities (C16 and phenol sample from Sigma Aldrich; Polycyclic Aromatic Hydrocarbons (PAH) mixture with Molecular Weight (MW) up to 300 Da given by Supelco EPA 525 PA H mix), the concentration of aromatics and aliphatics were measured. UV–Visible spectra of SOF samples dissolved in DCM and of soot dissolved in N-Methyl-2-pyrrolidonen (NMP) were measured on an HP 8453 Diode Array spectrophotometer. SOF fluorescence spectra were acquired on a HORIBA Scientific FluoroMax-Plus TCSPC spectrofluorometer. More details on the acquisition of fluorescence spectra are reported in Ref. [29]. MW distribution of SOF and soot samples were measured by size exclusion chromatography (SEC) by elution with NMP on a HPLC system HP1050 series equipped with an UV–Visible diode array detector measuring the absorbance signal at 350 nm. The MW distributions of SOF samples were measured on two different columns: a highly cross-linked "individual-pore" column and a Jordi Gel DVB Column for mass determination in the 100 – 2E4 u range and in the 2E3 - 4E8 u range, respectively. More details on SEC apparatus and conditions are reported in Ref. [30]. Soot samples were analyzed only on the Jordi GEL DVB column. The retention times of polystyrene and PAH standard species with known MW and of soot particles with known sizes (as determined by dynamic light scattering) were used to derive the MW calibration on both SEC columns [31]. Based on the calibration curve of each column the retention time abscissa of the SEC profiles was converted to MW. A Horiba XploRA Raman microscope system (Horiba Jobin Yvon, Japan) with an excitation wavelength of 532 nm (frequency doubled Nd:YAG-solid state laser, 25 mW) was used to measure the Raman spectrum of soot. The Raman spectra abscissa was calibrated with a silicon wafer by using the first-order Stokes Raman of pure Si at 520 cm^{-1}. Raman spectra were acquired between 900 and 3500 cm^{-1}. Care was taken to avoid carbon structure alteration by laser-induced heating effects modulating laser energy on the sample and acquisition parameters.

2.3. *Operating conditions*

Experiments were performed at 2000 and 3000 rpm both LL and HL to reflect the typical urban and extra-urban patterns of a commercial engine for passenger vehicle.

The start of injection (SOI) and start of spark (SOS) were set to ensure a stable combustion. The duration of injection (DOI) was modified to operate the engine with a lean air-to-fuel ratio (λ) with the aim to improve the performance and reduce the NO_x emissions. The tested operating conditions are summarized in Table 3. The indicated mean effective pressure (imep) and the coefficient of variation (COV) of imep are also shown. The COV imep has for all the conditions values below 2% revealing a good stability of the combustion.

Carbon emissions, such as CO, HC, and CO_2, are very low, below the detection limits of the analyzers, thus only NO_x was measured at the exhaust.

The engine run for nearly an hour at fixed operating condition to collect condensed exhaust samples. Three sampling at different days were realized. The sampling, sample treatment and preparation, and analytical measurements together contributed to a total uncertainty of the chemical and spectroscopic results of roughly 15%. During the test at fixed operating conditions, 10 acquisitions of 5 min each of the PSDs were performed. The PSD graphs presented in the experimental result section represent the average data of each acquisition. The variability among the different acquisitions is lower than 5%.

3. Experimental results

The experimental result section is divided in two parts. The first part deals with the physical characterization of the particles measured at exhaust. The second part, instead, is focused on the chemical characterization of the particles to better understand their nature.

3.1. *Physical particle characterization*

Fig. 3 shows the temporal evolution of the particle number concentration (N_p) measured during the tests carried out at 2000 rpm LL (Fig. 3-a) and 3000 rpm both LL and HL (Fig. 3-b). Particles are measured for all the test conditions except at 2000 rpm HL where their values are so low that are not detectable by the spectrometer. The graphs depict the

Table 3 – Operating conditions.

	Engine speed [rpm]	Throttle opening [%]	DOI [cad]	SOI [cad BTDC]	SOS [cad BTDC]	λ [–]	imep [bar]	COV imep [%]
2000 rpm -LL	2000	15	170	270	7.0	1.6	4.0	1.0
2000 rpm -HL	2000	95	225	260	11.6	1.5	5.5	1.2
3000 rpm -LL	3000	15	260	270	13.7	1.5	4.3	1.5
3000 rpm -HL	3000	95	240	352	10	1.6	5.7	1.6

effective values of N_p (dashed lines) and the filtered curves (solid lines) to highlight the oscillations of the particle concentration during the acquisitions.

Hydrogen fuel has no carbon atoms in its molecule so it should not emit particles. Therefore, it is presumable that the particles measured at exhaust are due to the lubricating oil. It is known in literature [32] that during the engine running, the oil accumulates in the combustion chamber near the cylinder surfaces and in the crevices. After a certain time, depending on the operating condition, the temperature in the chamber increases until it causes the oil to burn and/or oxidise thus contributing to the particle formation. It is worth noting that the particle emission is not constant over time, but it fluctuates.

It is, in fact, possible to distinguish several peaks of the same intensity and width at fixed engine operating condition. This behavior could be explained considering that the oil can accumulate and burn periodically. On this assumption, the higher the oil amount accumulated in the chamber that takes part to the combustion, the higher are the concentration peaks. Another aspect to consider in the cyclic entrainment of oil in the combustion chamber is the expansion of the rings. As shown in Fig. 3, the oil contribution to the particle emissions increases with the engine speed and increases as the load decreases. In the test conditions 2000 rpm – LL, N_p reaches a maximum value of 3.1×10^6 #/cm^3. At 3000 rpm, the particle concentration is higher with mean values of 1.0×10^7 #/cm^3 and 2.3×10^6 #/cm^3 at LL and HL, respectively. Moreover, it can be observed that also the frequency of the concentration peaks changes with the engine conditions. Less time elapses between the peaks at 3000 rpm with respect to the condition at 2000 rpm. This trend could be explained with the high frequency of formation of oil pool at high engine speed.

To analyze the impact of lubricating oil on the particle number and size, the PSDs were measured in the tested operating conditions, Fig. 4. Particles have dimeter ranging between 6 and 300 nm. The PSDs shape and intensity change

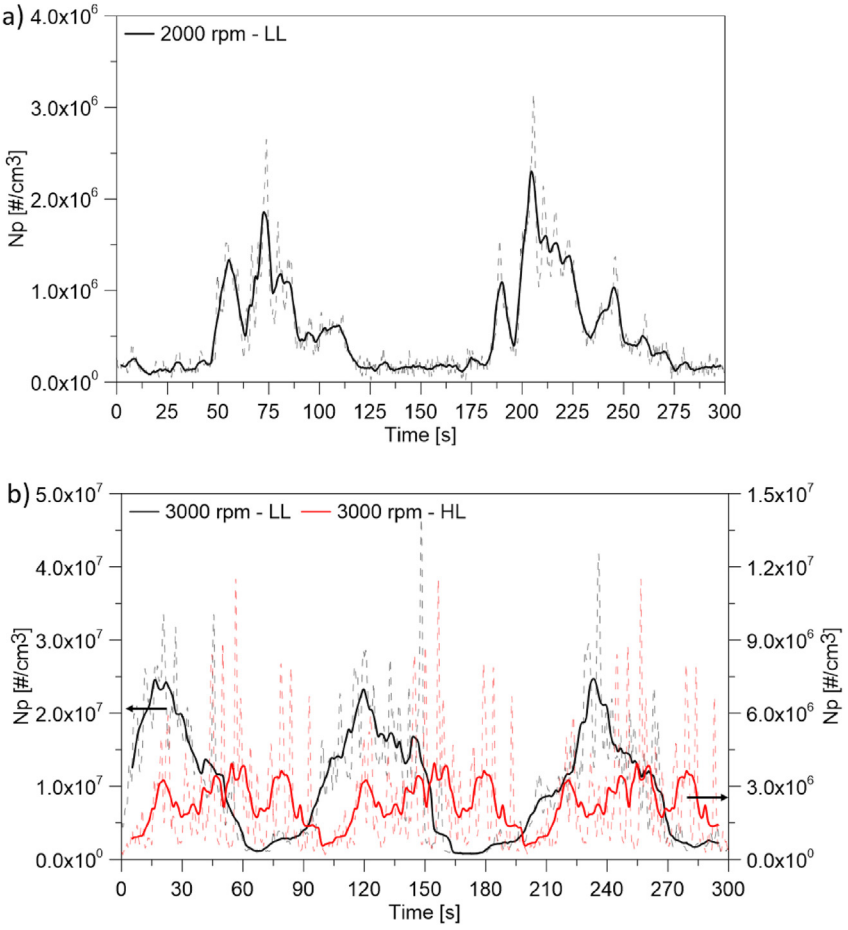

Fig. 3 – Temporal evolution of the particle number concentration measured at a) 2000 rpm – LL and b) 3000 rpm both LL and HL. The dashed lines represent the effective data while the solid lines are the fitting curves.

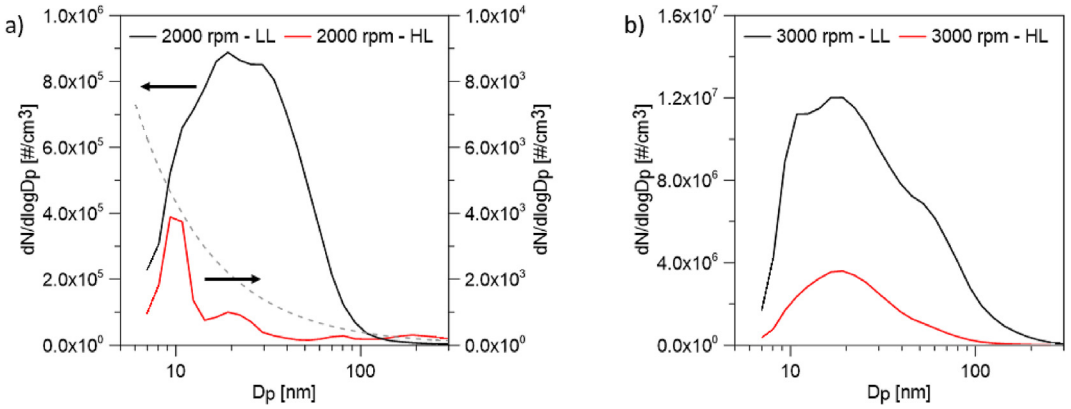

Fig. 4 – PSDs measured at a) 2000 rpm and b) 3000 rpm at both LL and HL. Dashed line is representative of the minimum limit value of the spectrometer.

according to the operating condition. At 2000 rpm LL, the PSD exhibits a peak of 8.9×10^5 #/cm^3 at 20 nm and a little hump of 6.6×10^5 #/cm^3 at 10 nm. On the other hand, the PSD at 2000 rpm – HL is within the limit values of the spectrometer, MIN, due to low signal to noise ratio so at this test point the conventional techniques do not provide relevant information on the particle emissions. At 3000 rpm – LL, the PSD shows a distinguishable nucleation mode (NM) reaching the value of 1.2×10^7 #/cm^3 at 10 nm and a less pronounced accumulation mode (AM) of 6.9×10^6 #/cm^3 at 53 nm. At 3000 rpm HL, the PSD is unimodal with a maximum value of 3.6×10^6 #/cm^3 at 20 nm. At both engine speeds, the particle number increases as the load decreases since more oil vapors are sucked in the combustion chamber because of the high depression downstream the throttle. In addition, as the load and, hence, the operation temperature increase, the piston and ring experience a great deformation thus guaranteeing a better seal. As a result, less amount of oil that can contribute to the particle formation is entrained in the cylinder. At fixed load, the particle concentration increases by about two orders of magnitude with the engine speed. In this case the dominant role is played by the higher combustion temperature resulting in the burning/oxidizing of the oil film on the cylinder surfaces when reached by the flame front.

To better highlight the role of the oil on the particle emissions, three size ranges were considered: 10–23 nm, which will be subject to the next emission regulation [33], 23–50 nm, representative of the NM, and >50 nm, typical of the AM. Fig. 5 depicts the N_p classified for the three dimensional range at the analyzed operating conditions. The extent of the particles varies according to the engine speed and load, evidencing the different role of the oil due to the environmental conditions realized at different operating conditions. At all test points, the larger amount of the particles, 48% at LL both 2000 and 3000 rpm, up to 57% at 3000 rpm HL, are smaller than 23 nm. These particles are due to the incomplete combustion and pyrolysis of high molecular weight hydrocarbons of the lubricating oil.

To take into account the effect of engine parameters on the particle emissions ascribable to the lubricating oil, the percentage particle variation due the load and speed was calculated and shown in Fig. 6. It arises that the speed changing account for 88% with respect to the 66% of the load highlighting that the major impact on the particle emissions is due to the engine speed. Therefore, it can be assumed that the major contribution to the particle emission is due to the incomplete combustion of the lubricant deposited on the cylinder surface at high temperature rather than the entrainment of oil vapor that can occur at low load.

3.2. *Chemical particle characterization*

Condensed exhausts were collected and analyzed using an array of chemical and spectroscopic techniques in order to

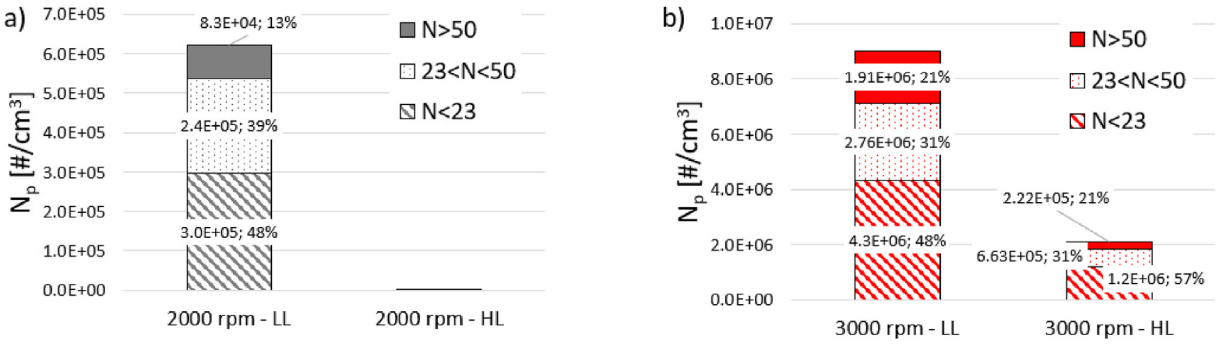

Fig. 5 – Particle number characterization with classification of the particles smaller than 23 nm, in the size range 23–50 nm and the particles larger than 50 nm at a) 2000 rpm and b) 3000 rpm at both LL and HL.

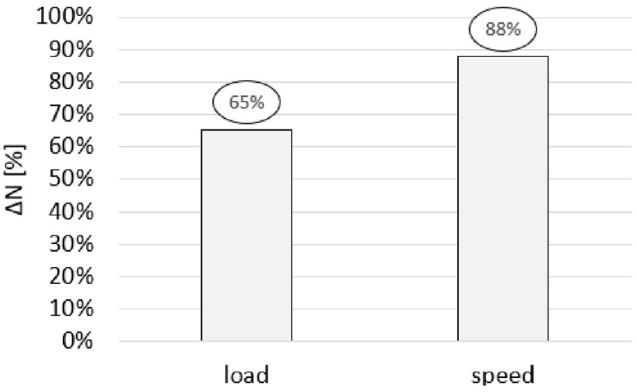

Fig. 6 – Percentage N_p variation due to the engine speed and load.

gain an in-depth understanding of the nature of the particles and species released from hydrogen-fueled engines.

The SOF was investigated by means of different techniques which allow a more comprehensive analysis of the nature of the particles emitted by hydrogen fueled engines. An overall description of SOF composition is given in Figs. 7 and 8 reporting the MW distributions measured with non-porous and not-mixed column, respectively, to detect particles and molecular species.

The MW distributions, obtained by off-line measurement technique, are focused on molecules and particles in the size range from 1 to 100 nm thus providing additional information with respect to those offered by on-line particle characterization performed with the EEPS (Fig. 4) in the particles size range from 6 to 560 nm. Moreover, due to the different sensitivity of the methods, SEC analysis allows to detect also low particle concentrations, as at 2000 rpm – HL, that are not measured through the EEPS. The distributions measured on the non-porous column are peaked at MW values

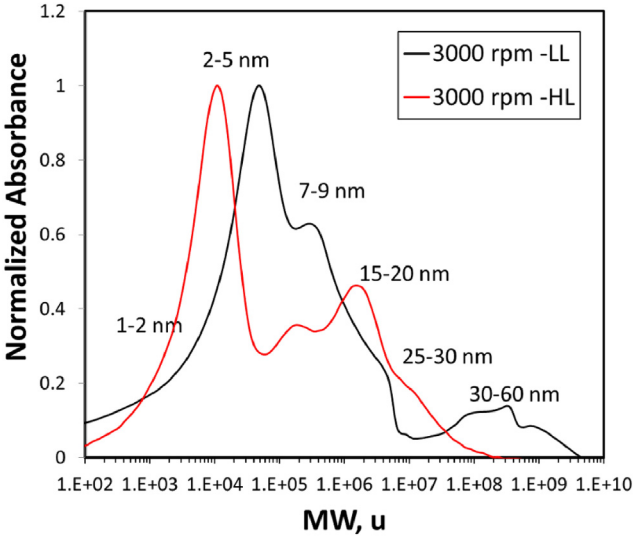

Fig. 7 – MW distribution profiles of the SOF samples from SEC with non-porous column of 3000 rpm samples at HL and LL, acquired with UV–Visible detector at 350 nm. The signals were normalized on the maximum value.

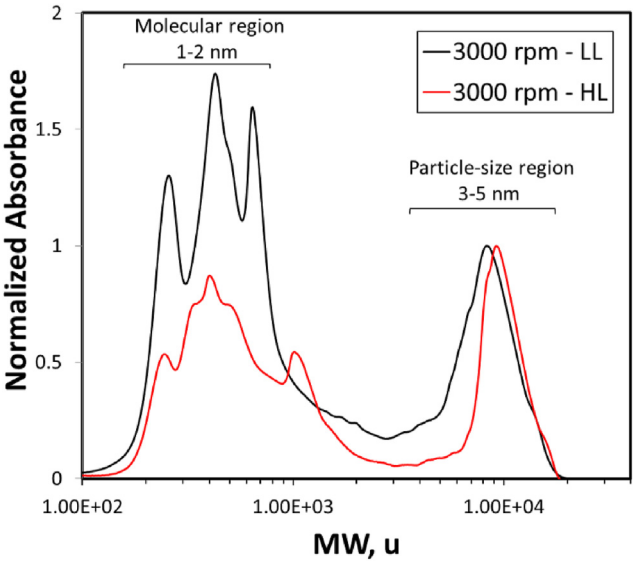

Fig. 8 – MW distribution profiles of the SOF samples from SEC with not mixed column of 3000 rpm samples at HL and LL, acquired with UV–Visible detector at 350 nm. The signals were normalized on the maximum value.

corresponding to particles with a dimension of 2–5 nm (assuming spherical particle and density value in a range between 1.2 and 1.8 g/cm^3 [34]) both for 3000 rpm-LL and 3000 rpm-HL samples. In comparison to the MW distribution measured for SOF collected at 2000 rpm at the same loads [15], samples collected at high engine speed are characterized by tails extending on larger MW values, corresponding to 25–30 nm for 3000 rpm-HL and 25–60 nm for 3000 rpm-LL. Independently on the engine speed, SOF samples at LL are characterized by the presence of heavier species in comparison to the corresponding samples at the same engine speed.

In the molecular region (Fig. 8), SOF sampled both at 3000 rpm and at 2000 rpm [15] exhibit peaks at similar MW values. The only striking difference among the samples regards the relative peak intensity ratio with the neat prevalence of the lower MW species mode for 3000 rpm-LL sample, indicating the highest presence of light molecular species absorbing at 350 nm.

Although the different detection techniques used to obtain the PSDs (Fig. 4) and the MW distributions (Figs. 7 and 8), a similar trend was observed in the same size range. Both methods, in fact, show the presence of more particles with larger diameter at higher engine speed. Furthermore, whatever the engine speed, the size of the particles decreases with the load.

To compare quantitatively the SOF emission, SEC profiles normalized for the sampling time are reported in Fig. 9. It is possible to observe the very high signal detected at 3000 rpm – LL. More details on the SOF composition can be retrieved by spectroscopic characterization. The UV–Visible spectra, normalized at a wavelength of 350 nm to better discriminate the presence of lighter as well as of heavier aromatic compounds, of all the SOF samples, with different engine speed and load, are reported in Fig. 10 and appear very similar in terms of spectral features. However, the highest abundance of

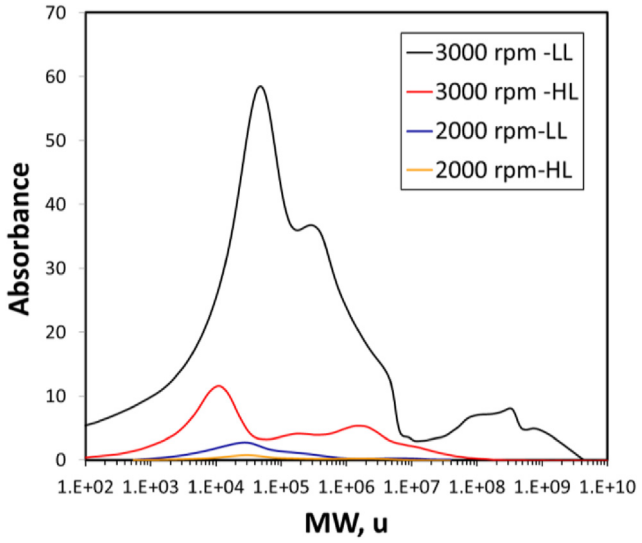

Fig. 9 – MW distribution profiles normalized for the sampling time of the SOF samples from SEC with non-porous column of SOF at HL and LL at 2000 and 3000 rpm acquired with UV–Visible detector at 350 nm.

light molecular species in the sample 3000 rpm-LL is confirmed by the higher absorption values in the UV region, whereas 2000 rpm-LL sample presents the highest absorbance values in the visible region highlighting the presence of large aromatic molecules. It is worth nothing that this result depicts not the absolute value rather the proportion between the lighter and heavier species for each operating condition.

The contour maps of the 3D fluorescence spectra of 3000 rpm SOF samples are reported in Fig. 11. As at 2000 rpm [15], SOF samples at 3000 rpm exhibit the most intense fluorescence signals between 300 and 400 nm when excited at 250 nm. However, at 3000 rpm-LL intense fluorescence signals are detected also when the sample is excited at higher

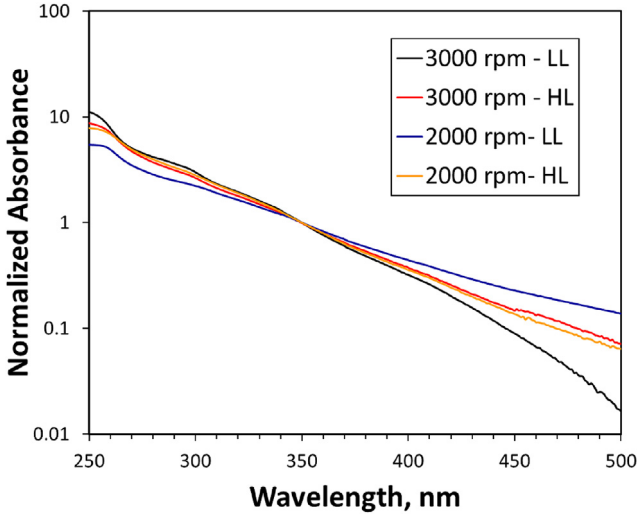

Fig. 10 – UV–visible absorption spectra normalized at 350 nm of SOF in DCM at HL and LL at 2000 and 3000 rpm in DCM.

excitation wavelength (up to 350 nm), indicating the presence of aromatic molecules with a higher MW.

Indeed, the fluorescence spectrum of a PAH mixture typically exhibits two main spectral regions: the first, caused by two- and three-ring PAH, is from 300 to 350 nm, and the second, caused mostly by bigger PAH (3–6 rings), is between 350 and 500 nm [35]. As the excitation wavelength increases only species with a higher number of rings are excited. The interpretation of the emission spectrum of aromatic mixtures is made simpler by synchronous fluorescence since each peak essentially corresponds to a single component or class of components, allowing for the possibility of a simplified study of multicomponent PAH mixtures [36]. As the ring number rises, synchronous signals occur at longer wavelengths.

In Fig. 12 the synchronous fluorescence spectra of the SOF samples at 3000 and 2000 rpm, with different load are reported for comparison. The spectra indicate that 3000 rpm-LL and 2000 rpm–LL samples are characterized by a PAH distribution richer in species with 3–6 aromatic rings, that are species highly fluorescent in the visible, whereas samples at HL have a PAH distribution shifted at lower masses. In particular, the sample 2000 rpm –LL presents the higher contribution of PAHs with more than seven rings, consistently with its UV–Visible spectrum (Fig. 10).

An indication of the PAH concentration inside the SOF samples has been done with GC-MS analysis and is reported in Fig. 13. It is worth underlining that only about 60–70% of the weight of the SOF samples was detected and identified by GC-MS. The remaining part, characterized by a MW higher than 300 u and thus undetectable by GC-MS, was investigated by spectroscopic techniques and SEC, even if aliphatic portion is weekly absorbing at 350 nm (SEC) and fluorescing.

Aromatic species are mainly constituted of oxy-PAHs and alkyl-PAHs. The aromatic species are submerged by the aliphatic species coming from oil and they were detected only by ion extraction. Only in the SOF sample at 3000 rpm – LL peaks due to aromatic species arise clearly in the chromatogram and their percentage of mass concentration was calculated to be 12.5%. The identification of these species has caused for concern since, despite their extremely low concentration, they exhibit extremely high levels of toxicity and mutagenicity, surpassing even those of unsubstituted PAH [37]. Aliphatic species account for about 90% of SOF and although less toxic than PAHs, their contribution to contamination of soil bacterial communities is not negligible [38].

It has been demonstrated in our previous work [15] that the incomplete combustion of the organic components in the lubricating oil and the breakdown of the carbon can be responsible for these pollutants. These findings showed that the presence of PAHs and nanoparticles was a constant throughout engine operation and characterized the exhaust of a hydrogen-fueled engine at various engine speeds and loads. The different behavior with load at 2000 and 3000 rpm can be ascribed to the different environmental condition encountered by the oil in the combustion chamber. At 2000 rpm-HL PAH and nanoparticles are formed in very low amounts. At 2000 rpm-LL aromatic species with more than 7 rings are present but their concentration and the experienced temperature are not enough to convert them in soot. In particular, at low engine speed the temperature is lower inhibiting the

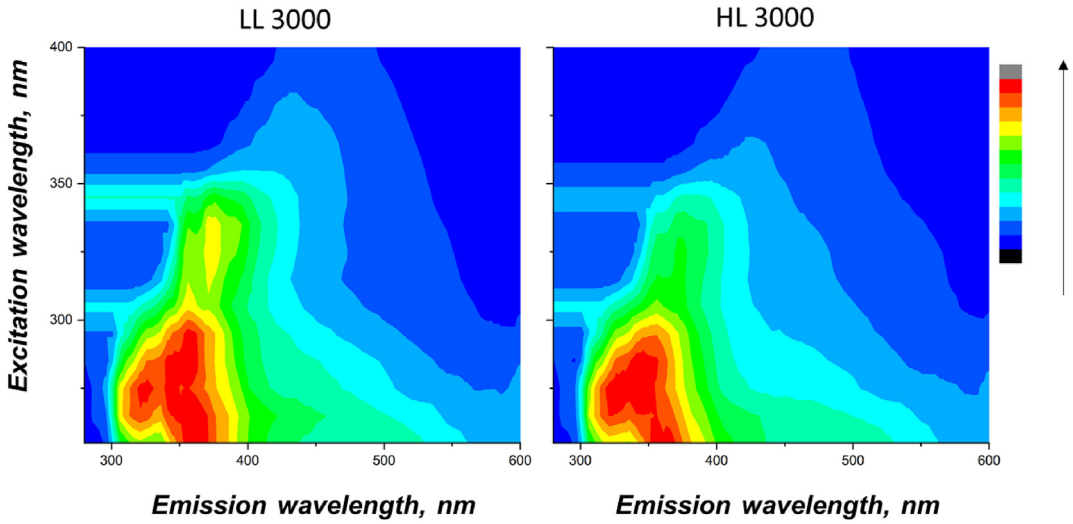

Fig. 11 – Contour map of the three-dimensional fluorescence spectra of SOF in DCM at LL and HL at 3000 rpm in DCM.

evaporation even of the lighter compounds of the oil conversely enhancing the condensation of the oil vapor.

It is worth to underline that soot, i.e., a fraction not soluble in DCM, was found only at 3000 rpm –LL and 3000 rpm –HL conditions. In both cases, it was not possible to perform gravimetric estimation of soot amount however the filters appear grey.

In Fig. 14 the MW distributions of soot and SOF samples are reported and contrasted with the normalized PSDs measured by the EEPS. PSDs have to be compared with both SOF and soot samples, which have been separated for analytical convenience when both are present. Soot and SOF MW distributions are peaked at MW values corresponding to particles with a dimension of 2–10 nm. The soot at 3000 rpm – LL presents a tail extending toward aggregates larger than 100 nm. This result is in accordance with the physical characterization of the particles. The normalized PSDs, in fact, show at both LL and HL the presence of particles smaller than 10 nm and a hump around 100 nm at 3000 rpm - LL. This is consistent with the higher presence of PAH species in the SOF samples at 3000 rpm –LL since a large amount of aromatics increases the formation of nucleated particles that rapidly grow and coagulate to form larger aggregates.

It was possible to measure the Raman spectrum of the soot sample 3000 rpm- LL, reported in Fig. 15. Indeed, only in this condition soot amount was enough on the filter to perform this analysis. In the first-order Raman region, between 1000 and 1800 cm^{-1}, the two characteristic peaks of carbon materials, i.e. the G (around 1600 cm^{-1}) and D (around 1350 cm^{-1}) can be observed. A low fluorescence background underlying the peak can be also observed, which is indicative of low hydrogen content (H/C atomic ratio <0.2) [39]. The second-order region, between 2000 and 3500 cm-1, has less intense and poorly defined bands that are indicative of disordered carbons [40].

Spectrum deconvolution with five curves, as described in Ref. [41], allows to calculate the ratio between the intensities (I) of the D and G peaks, i.e. I(D)/I(G) ratio, to derive the size of the aromatic layer length [42]. It was found that the I(D)/I(G) ratio was 0.95 corresponding to an aromatic length of 1.23 nm.

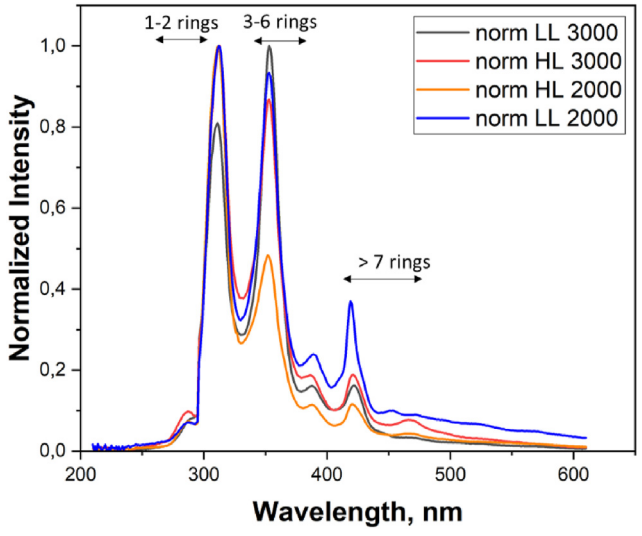

Fig. 12 – Height normalized synchronous fluorescence spectra (Δλ = 10 nm) of SOF in DCM at HL and LL at 2000 and 3000 rpm in DCM.

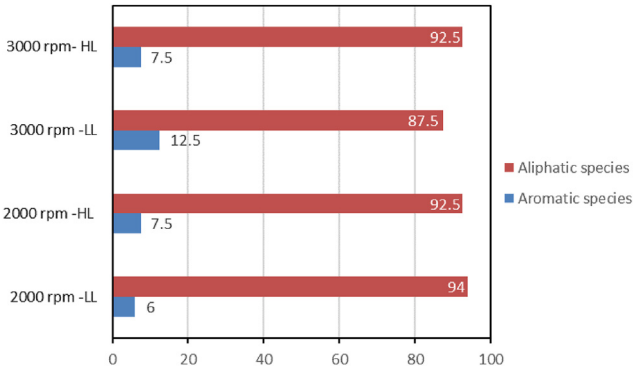

Fig. 13 – Percent mass concentration of aliphatic and aromatic species of SOF at HL and LL at 2000 and 3000 rpm as detected by GC-MS.

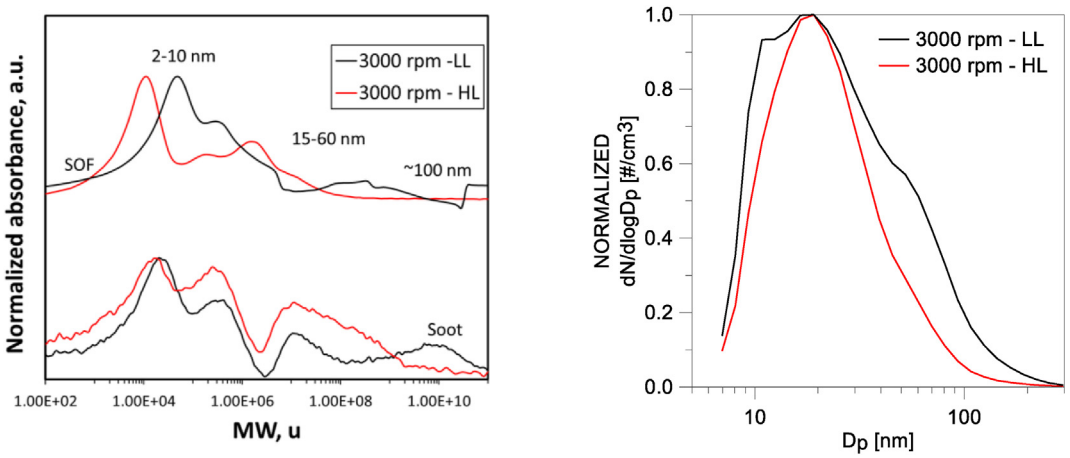

Fig. 14 – Height normalized MW distribution profiles of the soot and SOF samples from SEC analysis at 3000 rpm at HL and LL, acquired with UV–Visible detector at 350 nm compared with PSDs measured by EEPS.

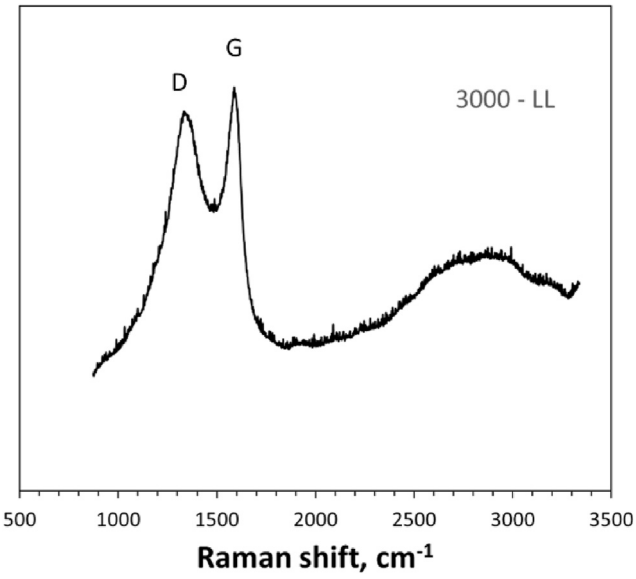

Fig. 15 – Raman spectrum of soot sample collected at 3000 rpm – LL.

Differently from SOF, soot is formed only at the high engine speed, i.e. at higher temperatures, and its contribute increases as the load decreases. The formed soot is comparable in terms of nanostructures to a mature soot having low hydrogen content [41] and a relatively high extension of the aromatic plane. The results demonstrate that beside PAHs and small particles soluble in DCM also larger particles and aggregates are also formed when the lubricant oil partially oxidizes leading to a not negligible particle formation at higher temperature, i.e. at higher engine speed.

4. Conclusions

This research study presents the impact of the lubricating oil and of the operating conditions on the particles emitted by a single cylinder, small displacement SI engine fed with hydrogen injected in direct mode. The investigation was carried out at different engine speeds and loads to evaluate the interaction between the environmental conditions and the lube oil during the combustion process to better point out the critical point on the particle emissions. The novelty of this manuscript consists in the use of complementary techniques, for both physical and chemical characterization of the particles, which allow a more comprehensive analysis of the role of the lube oil. Particle number and size were measured on the diluted exhaust during the engine running. Spectroscopic and chemical analysis were applied off-line on the condensed exhaust and the particles collected on a filter.

The main results can be summarized as follow:

- The particle emission measured through physical techniques is not constant over time, but it fluctuates due to the oil that can accumulate in the chamber and burns periodically.
- The extent of the particle emissions varies according to the engine speed and load, evidencing the different role of the oil due to the environmental conditions realized at different operating conditions.
- PAHs and nanoparticles have been found in the exhausts of a hydrogen-fueled engine at various engine speeds and loads, thus their emission is independently from the engine operation
- Oil incomplete combustion leads to soot formation only at higher temperatures, i.e. at higher engine speed.

The topic of lubricating oil for hydrogen-fueled engines is particularly relevant considering the effects of long-term use of hydrogen on the engine materials. Anyway, these results highlighted that a deepen awareness on the emission of the particles due to the lube oil in the atmosphere but also the impact of the condensed exhaust on the soil pollution is essential. Therefore, it can be argued the importance to understand the mechanisms of oil transformation, such as oxidation and dissociation, leading to the particle formation.

This analysis allows to have a deep insight on the components of the oil that plays the major role on the particle

formation thus offering important information for a proper optimization of the oil formulation. Moreover, in light of the high particle concentration emitted at some operating conditions also by the hydrogen fueled engines, it cannot be ruled out the use of specific after-treatment systems not only to abate the high NOx emissions typical of hydrogen combustion but also a proper device for particles, taking into account their nature and also the specific composition of the exhaust to guarantee an effective zero impact on the atmosphere and soil.

CRediT authorship contribution statement

Barbara Apicella: Methodology, Investigation, Data curation, Writing-original draft, Visualization. **Francesco Catapano**: Methodology, Investigation. **Silvana Di Iorio**: Conceptualization, Methodology, Investigation, Data curation, Writing-original draft, Visualization. **Agnese Magno**: Conceptualization, Methodology, Investigation, Data curation, Writing-original draft, Visualization. **Carmela Russo**: Data curation, Writing-original draft, Visualization. **Paolo Sementa**: Methodology, Investigation. **Antonio Tregrossi**: Methodology, Investigation. **Bianca Maria Vaglieco**: Writing-review & editing, Supervision.

Declaration of competing interest

The authors declare that they have no known competing financial interests or personal relationships that could have appeared to influence the work reported in this paper.

Acknowledgments

Authors thank Carlo Rossi and Bruno Sgammato for the engine assessment and for the support in the experimental activity.

REFERENCES

[1] 2050 long-term strategy n.d. https://climate.ec.europa.eu/eu-action/climate-strategies-targets/2050-long-term-strategy_en. [Accessed 27 March 2023].
[2] Di Iorio S, Catapano F, Magno A, Sementa P, Vaglieco BM. The potential of ethanol/methanol blends as renewable fuels for DI SI engines. Energies 2023;16:2791. https://doi.org/10.3390/en16062791.
[3] Catapano F, Iorio S Di, Magno A, Sementa P, Vaglieco BM. Effect of ethanol blends , E10 , E25 and E85 on sub-23 nm particle emissions and their volatile fraction at exhaust of a high-performance GDI engine over the WLTC. Fuel 2022;327:125184. https://doi.org/10.1016/j.fuel.2022.125184.
[4] Catapano F, Di Iorio S, Magno A, Vaglieco BM. Effect of fuel quality on combustion evolution and particle emissions from PFI and GDI engines fueled with gasoline, ethanol and blend, with focus on 10–23 nm particles. Energy 2022;239:122198. https://doi.org/10.1016/j.energy.2021.122198.
[5] Awad OI, Mamat R, Ali OM, Sidik NAC, Yusaf T, Kadirgama K, et al. Alcohol and ether as alternative fuels in spark ignition engine: a review. Renew Sustain Energy Rev 2018;82:2586–605. https://doi.org/10.1016/j.rser.2017.09.074.
[6] Ortiz-Imedio R, Ortiz A, Ortiz I. Comprehensive analysis of the combustion of low carbon fuels (hydrogen, methane and coke oven gas) in a spark ignition engine through CFD modeling. Energy Convers Manag 2022;251:114918. https://doi.org/10.1016/j.enconman.2021.114918.
[7] Onorati A, Payri R, Vaglieco BM, Agarwal AK, Bae C, Bruneaux G, et al. The role of hydrogen for future internal combustion engines. Int J Engine Res 2022;23:529–40. https://doi.org/10.1177/14680874221081947.
[8] Wilberforce T, Olabi AG, Monopoli D, Dassisti M, Sayed ET, Abdelkareem MA. Design optimization of proton exchange membrane fuel cell bipolar plate. Energy Convers Manag 2023;277:116586. https://doi.org/10.1016/j.enconman.2022.116586.
[9] Rasul MG, Hazrat MA, Sattar MA, Jahirul MI, Shearer MJ. The future of hydrogen: challenges on production, storage and applications. Energy Convers Manag 2022;272:116326. https://doi.org/10.1016/j.enconman.2022.116326.
[10] Lee S, Kim Y, Lee J, Kim K, Lee S, Min K, et al. Energy and exergy analyses of hydrogen-fueled spark ignition engine with various air excess ratios and ignition timings. Fuel 2023;349:128588. https://doi.org/10.1016/j.fuel.2023.128588.
[11] Marwaha A, Subramanian KA. Experimental investigation on effect of misfire and postfire on backfire in a hydrogen fuelled automotive spark ignition engine. Int J Hydrogen Energy 2023;48:24139–49. https://doi.org/10.1016/j.ijhydene.2023.03.155.
[12] Duan X, Xu L, Xu L, Jiang P, Gan T, Liu H, et al. Performance analysis and comparison of the spark ignition engine fuelled with industrial by-product hydrogen and gasoline. J Clean Prod 2023. https://doi.org/10.1016/j.jclepro.2023.138899.
[13] Yosri MR, Palulli R, Talei M, Mortimer J, Poursadegh F, Yang Y, et al. Numerical investigation of a large bore, direct injection, spark ignition, hydrogen-fuelled engine. Int J Hydrogen Energy 2023;48:17689–702. https://doi.org/10.1016/j.ijhydene.2023.01.228.
[14] Di Iorio S, Catapano F, Magno A, Sementa P, Vaglieco BM. Investigation on sub-23 nm particles and their volatile organic fraction (VOF) in PFI/DI spark ignition engine fueled with gasoline, ethanol and a 30 %v/v ethanol blend. J Aerosol Sci 2021;153:105723. https://doi.org/10.1016/j.jaerosci.2020.105723.
[15] Apicella B, Catapano F, Di Iorio S, Magno A, Russo C, Sementa P, et al. Comprehensive analysis on the effect of lube oil on particle emissions through gas exhaust measurement and chemical characterization of condensed exhaust from a DI SI engine fueled with hydrogen. Int J Hydrogen Energy 2023;48:22277–87. https://doi.org/10.1016/j.ijhydene.2023.03.112.
[16] Brandenberger S, Mohr M, Grob K, Neukom HP. Contribution of unburned lubricating oil and diesel fuel to particulate emission from passenger cars. Atmos Environ 2005;39:6985–94. https://doi.org/10.1016/j.atmosenv.2005.07.042.
[17] Carbone S, Timonen HJ, Rostedt A, Happonen M, Rönkkö T, Keskinen J, et al. Distinguishing fuel and lubricating oil combustion products in diesel engine exhaust particles. Aerosol Sci Technol 2019;53:594–607. https://doi.org/10.1080/02786826.2019.1584389.
[18] Pirjola L, Karjalainen P, Heikkila J, Saari S, Tzamkiozis T. Effects of fresh lubricant oils on particle emissions emitted by a modern gasoline direct injection passenger car. Environ Sci Technol 2015;49:3644–52. https://doi.org/10.1021/es505109u.

[19] Kleeman MJ, Riddle SG, Robert MA, Jakober CA. Lubricating oil and fuel contributions to particulate matter emissions from light-duty gasoline and heavy-duty diesel vehicles. Environ Sci Technol 2008;42:235–42. https://doi.org/10.1021/es071054c.
[20] Worton DR, Isaacman G, Gentner DR, Dallmann TR, Chan AWH, Ruehl C, et al. Lubricating oil dominates primary organic aerosol emissions from motor vehicles. Environ Sci Technol 2014;48:3698–706. https://doi.org/10.1021/es405375j.
[21] Lähde T, Giechaskiel B, Martini G, Howard K, Jones J, Ubhi S. Effect of lubricating oil characteristics on solid particle number and CO2 emissions of a Euro 6 light-duty compressed natural gas fuelled vehicle. Fuel 2022;324:124763. https://doi.org/10.1016/j.fuel.2022.124763.
[22] Hamnas A, Unnikrishnan G. Bio-lubricants from vegetable oils: characterization, modifications, applications and challenges – review. Renew Sustain Energy Rev 2023;182:113413. https://doi.org/10.1016/j.rser.2023.113413.
[23] Singh AP, Pal A, Agarwal AK. Comparative particulate characteristics of hydrogen, CNG, HCNG, gasoline and diesel fueled engines. Fuel 2016;185:491–9. https://doi.org/10.1016/j.fuel.2016.08.018.
[24] Thawko A, Eyal A, Tartakovsky L. Experimental comparison of performance and emissions of a direct-injection engine fed with alternative gaseous fuels. Energy Convers Manag 2022;251:114988. https://doi.org/10.1016/j.enconman.2021.114988.
[25] Thawko A, Tartakovsky L. The mechanism of particle formation in non-premixed hydrogen combustion in a direct-injection internal combustion engine. Fuel 2022;327:125187. https://doi.org/10.1016/j.fuel.2022.125187.
[26] Di Iorio S, Sementa P, Vaglieco BM, Catapano F. An experimental investigation on combustion and engine performance and emissions of a methane-gasoline dual-fuel optical engine. SAE Tech Pap 2014;1. https://doi.org/10.4271/2014-01-1329.
[27] Johnson T, Caldow R, Pöcher A, Mirme A, Kittelson D. A new electrical mobility particle sizer spectrometer for engine exhaust particle measurements. SAE Tech Pap 2004;2004. https://doi.org/10.4271/2004-01-1341.
[28] Apicella B, Mancaruso E, Russo C, Tregrossi A, Maddalena M, Ciajolo A, et al. E ff ect of after-treatment systems on particulate matter emissions in diesel engine exhaust. Exp Therm Fluid Sci 2020;116:110107. https://doi.org/10.1016/j.expthermflusci.2020.110107.
[29] Russo C, Carpentieri A, Tregrossi A, Ciajolo A, Apicella B. Blue, green and yellow carbon dots derived from pyrogenic carbon: structure and fluorescence behaviour. Carbon N Y 2023;201:900–9. https://doi.org/10.1016/j.carbon.2022.09.062.
[30] Russo C, Ciajolo A, Stanzione F, Tregrossi A, Apicella B. Separation and online optical characterization of fluorescent components of pyrogenic carbons for carbon dots identification. Carbon N Y 2023;209:118009. https://doi.org/10.1016/j.carbon.2023.118009.
[31] Apicella B, Ciajolo A, Tregrossi A, M TJ, Herod AA, Kandiyoti R. Size exclusion chromatography of particulate produced in fuel-rich combustion of different fuels. Energy Fuels 2003;17:565–70. https://doi.org/10.1021/ef020149r.
[32] Thawko A, Yadav H, Eyal A, Shapiro M, Tartakovsky L. Particle emissions of direct injection internal combustion engine fed with a hydrogen-rich reformate. Int J Hydrogen Energy 2019;44:28342–56. https://doi.org/10.1016/j.ijhydene.2019.09.062.
[33] Samaras Z, Rieker M, Papaioannou E, van Dorp WF, Kousoulidou M, Ntziachristos L, et al. Perspectives for regulating 10 nm particle number emissions based on novel measurement methodologies. J Aerosol Sci 2022;162:105957. https://doi.org/10.1016/j.jaerosci.2022.105957.
[34] D'Anna A, Ciajolo A, Alfè M, Apicella B, Tregrossi A. Effect of fuel/air ratio and aromaticity on the molecular weight distribution of soot in premixed n-heptane flames. Proc Combust Inst 2009;32 I:803–10. https://doi.org/10.1016/j.proci.2008.06.198.
[35] Berlman IB. Fluorescence spectra of aromatic molecules. New York and London: Academic P.; 1971.
[36] Vo-Dinh T. Multicomponent analysis by synchronous luminescence spectrometry. Anal Chem 1978;50:396–401. https://doi.org/10.1021/ac50025a010.
[37] Krzyszczak A, Czech B. Occurrence and toxicity of polycyclic aromatic hydrocarbons derivatives in environmental matrices. Sci Total Environ 2021;788. https://doi.org/10.1016/j.scitotenv.2021.147738.
[38] Liu Y, Ding A, Sun Y, Xia X, Zhang D. Impacts of n-alkane concentration on soil bacterial community structure and alkane monooxygenase genes abundance during bioremediation processes. Front Environ Sci Eng 2018;12. https://doi.org/10.1007/s11783-018-1064-5.
[39] Casiraghi C, Piazza F, Ferrari AC, Grambole D, Robertson J. Bonding in hydrogenated diamond-like carbon by Raman spectroscopy. Diam Relat Mater 2005;14:1098–102. https://doi.org/10.1016/j.diamond.2004.10.030.
[40] Baratta GA, Mennella V, Brucato JR, Colngeli L, Leto G, Palumbo ME, et al. Raman spectroscopy of ion-irradiated interplanetary carbon dust analogues. J Raman Spectrosc 2004;35:487–96. https://doi.org/10.1002/jrs.1169.
[41] Russo C, Ciajolo A. Effect of the flame environment on soot nanostructure inferred by Raman spectroscopy at different excitation wavelengths. Combust Flame 2015;162:2431–41. https://doi.org/10.1016/j.combustflame.2015.02.011.
[42] Ferrari AC, Robertson J. Resonant Raman spectroscopy of disordered, amorphous, and diamondlike carbon. Phys Rev B 2001;64. https://doi.org/10.1103/PhysRevB.64.075414.

Abbreviations

AM	Accumulation mode
CO_2	Carbon dioxide
CNG	Compressed natural gas
COV	Coefficient of Variance
DCM	Dichloromethane
DI	Direct Injection
DOI	Duration of Injection
EEPS	Engine Exhaust Particle Spectrometer
ETU	Engine Timing Unit
GC/MS	Gas Chromatography Mass Spectrometry
HCNG	Hydrogen-CNG mixtures
HL	High load
ICE	Internal Combustion Engine
IMEP	Indicated Mean Effective Pressure
λ	Excess air ratio
LL	Low load
MW	Molecular Weight
NM	Nucleation mode
NMP	N-methyl pyrrolidone
N_p	Particle number concentration
PAH	Polycyclic Aromatic Hydrocarbons
PFI	Port fuel injection
PSD	Particle Size Distribution
SD	Single Diluter
SEC	Size Exclusion Chromatography
SI	Spark Ignition
SOF	Soluble Organic Fraction
SOI	Start of Injection
SOS	Start of Spark